The Astrophysical Journal Letters, 831:L3 (7pp), 2016 November 1 doi:10.3847/2041-8205/831/1/L3

NEUTRON-CAPTURE ELEMENT ABUNDANCES IN MAGELLANIC CLOUD PLANETARY NEBULAE*

A. L. Mashburn[1], N. C. Sterling[1], S. Madonna[2], Harriet L. Dinerstein[3], I. U. Roederer[4,5], and T. R. Geballe[6]
[1] Department of Physics, University of West Georgia, 1601 Maple Street, Carrollton, GA 30118, USA; awhite15@my.westga.edu, nsterlin@westga.edu
[2] Instituto de Astrofísica de Canarias, Departamento Astrofísica, Universidad de La Laguna, E-38206 La Laguna, Tenerife, Spain; smadonna@iac.es
[3] Department of Astronomy, University of Texas, 2515 Speedway, C1400, Austin, TX 78712-1205, USA; harriet@astro.as.utexas.edu
[4] Department of Astronomy, University of Michigan, 1085 South University Avenue, Ann Arbor, MI 48109, USA; iur@umich.edu
[5] Joint Institute for Nuclear Astrophysics and Center for the Evolution of the Elements (JINA-CEE), USA
[6] Gemini Observatory, 670 N. A'ohoku Place, Hilo, HI 96720, USA; tgeballe@gemini.edu
Received 2016 September 8; revised 2016 October 3; accepted 2016 October 8; published 2016 October 24

ABSTRACT

We present near-infrared spectra of 10 planetary nebulae (PNe) in the Large and Small Magellanic Clouds (LMC and SMC), acquired with the FIRE and GNIRS spectrometers on the 6.5 m Baade and 8.1 m Gemini South Telescopes, respectively. We detect Se and/or Kr emission lines in eight of these objects, the first detections of *n*-capture elements in Magellanic Cloud PNe. Our abundance analysis shows large *s*-process enrichments of Kr (0.6–1.3 dex) in the six PNe in which it was detected, and Se is enriched by 0.5–0.9 dex in five objects. We also estimate upper limits to Rb and Cd abundances in these objects. Our abundance results for the LMC are consistent with the hypothesis that PNe with 2–3 $M_{\odot}$ progenitors dominate the bright end of the PN luminosity function in young gas-rich galaxies. We find no significant correlations between *s*-process enrichments and other elemental abundances, central star temperature, or progenitor mass, though this is likely due to our small sample size. We determine S abundances from our spectra and find that [S/H] agrees with [Ar/H] to within 0.2 dex for most objects, but is lower than [O/H] by 0.2–0.4 dex in some PNe, possibly due to O enrichment via third dredge-up. Our results demonstrate that *n*-capture elements can be detected in PNe belonging to nearby galaxies with ground-based telescopes, allowing *s*-process enrichments to be studied in PN populations with well-determined distances.

Key words: infrared: general – Magellanic Clouds – nuclear reactions, nucleosynthesis, abundances – planetary nebulae: general – stars: AGB and post-AGB

Supporting material: machine-readable table

1. INTRODUCTION

Emission lines of neutron (*n*)-capture elements (atomic number $Z > 30$) were first identified in a planetary nebula (PN) in 1994 (Péquignot & Baluteau 1994), and since have been detected in more than 100 Galactic PNe (e.g., Sharpee et al. 2007; Sterling & Dinerstein 2008; García-Rojas et al. 2015). Trans-iron elements can be produced by slow *n*-capture nucleosynthesis (the "*s*-process") in asymptotic giant branch (AGB) stars, and transported to the stellar envelope by third dredge-up (TDU) before being expelled via stellar winds and PN ejection (Karakas & Lattanzio 2014). Comparisons of empirically determined *s*-process enrichments in PNe to theoretical predictions provide valuable constraints to models of AGB nucleosynthesis (Karakas et al. 2009; Sterling et al. 2016).

To date, nebular *n*-capture element abundance determinations have almost exclusively been limited to Galactic PNe, whose primarily statistical distances can have substantial uncertainties (though improved calibrations to statistical distance scales show promise for better accuracies; Frew et al. 2016 and references therein). Because of the uncertain distances, it has not been possible to study *s*-process enrichments along the PN luminosity function (PNLF; Jacoby 1989)—which prevents robust estimates of the fraction of PNe that are *s*-process enriched (Sterling & Dinerstein 2008)—or as a function of initial stellar mass.

Extragalactic PNe do not suffer from the distance uncertainties that plague Galactic objects. However, this advantage comes at a cost, as the large distances of these PNe render the detection of faint emission lines difficult. Nevertheless, it is possible to detect *n*-capture elements in Local Group PNe with sufficiently large-aperture telescopes.

The Large and Small Magellanic Clouds (LMC and SMC) are optimal targets for such a study, given their relative proximity (50 and 60 kpc, respectively; Keller & Wood 2006), minimal foreground extinction, and relatively well-studied PN populations. A significant fraction of LMC and SMC PNe have been identified (Reid 2014; Drašković et al. 2015), and elemental abundances have been determined in a large number of these objects (e.g., Leisy & Dennefeld 2006 and references therein). In addition, progenitor star masses have been estimated for some PNe in these galaxies (Villaver et al. 2003, 2004, 2007).

In this Letter, we present the detection of near-infrared [Kr III] and [Se IV] emission lines in 10 bright LMC and SMC PNe. To our knowledge, these are the first detections of *n*-capture elements in extragalactic PNe other than the Sagittarius Dwarf (Wood et al. 2006; Otsuka et al. 2011).

2. OBSERVATIONS AND REDUCTIONS

In Table 1, we provide an observing log and nebular and stellar parameters for our sample. Nine of the 10 PNe were observed with the Folded-Port InfraRed Echellette (FIRE) spectrograph (Simcoe et al. 2013) on the 6.5 m Baade Telescope at Las Campanas Observatory. We used a 0.″75 slit width to provide a resolution $R = 4800$ in echelle mode, covering the spectral range 0.83–2.45 μm. Because the targets have diameters comparable to or smaller than the slit width, light loss primarily occurred due to seeing conditions, which were typically less than 1″ but ranged from 2″–4″ for

* This paper includes data obtained with the 6.5-m Magellan Telescopes located at Las Campanas Observatory, Chile, and with the Gemini-South Telescope at Cerro Pachon, Chile.

Table 1
Observing Log and Nebular Properties

Galaxy	PN Name	Date Observed	Inst.	Int. Time (s)	T_e[O III] (10^3 K)	n_e (10^3 cm^{-3})	$c_{H\beta}$	m_{5007}[a]	Log C/O[b]	Log N/O	T_{eff}[c] (10^3 K)	M_{init}[c] ($M_\odot$)
LMC	SMP 6	2013-01-22	FIRE	4600	13.3	11.8	0.04	15.53	…	−0.99	140.0	…
	SMP 47	2013-01-22	FIRE	2100	14.7	4.8	0.42	15.28	0.37	0.45	150.0	…
	SMP 62	2006-08-16	GNIRS	1120	15.9	3.4	0.06	14.67	−0.85	−0.26	100.0	…
	SMP 63	2013-01-21	FIRE	3840	11.9	7.4	0.11	15.17	0.01	−0.34	38.8	1.5–2.0
	SMP 73	2013-08-12	FIRE	5600	11.7	4.5	0.34	14.93	0.18	−0.63	135.0	…
	SMP 85	2013-01-21	FIRE	2400	11.7	31.4	0.42	16.15	0.64	−0.74	46.0	…
	SMP 99	2013-01-21	FIRE	4320	12.7	2.29	0.35	14.98	0.28	−0.60[d]	124.0	…
SMC	SMP 15	2013-08-11	FIRE	5400	12.0	5.0	0.04	15.67	0.12	−0.37	58.0	…
	SMP 17	2013-08-12	FIRE	8000	12.2	2.9	0.06	15.52	0.19	−0.83	58.4	1.0
	SMP 20	2013-08-11	FIRE	7200	13.8	3.9	0.0	16.12	0.51	−0.79	86.5	1.0–1.5
	SMP 20	2006-08-16	GNIRS	1120								

Notes. Nebular temperatures, densities, extinction coefficients, N/O, and (unless specified) C/O abundances are from Shaw et al. (2010, hereafter S10) for SMP 17 and 20, Tsamis et al. (2003, T03) for SMP 63, Meatheringham & Dopita (1991, MD91) for SMP 99, and Leisy & Dennefeld (2006, LD06) for the remaining PNe.
[a] Apparent [O III] 5007 magnitudes computed from absolute fluxes (corrected for foreground extinction) measured with the *Hubble Space Telescope* (Stanghellini et al. 2003; Shaw et al. 2006), with the exceptions of SMP 85 and SMP 99 (LD06), using the relation $m_{5007} = -2.5 \log F_{5007} - 13.74$ (Jacoby 1989).
[b] C/O abundances are from the references above, with the exceptions of SMP 62 and SMP 17 (Aller et al. 1987), SMP 85 (Dopita et al. 1994), and SMP 15 and SMP 20 (Stanghellini et al. 2009).
[c] References for central star temperatures: SMP 62 (Aller et al. 1987), SMP 85 (Dopita et al. 1994), SMP 63 (Villaver et al. 2003), SMP 17 and 20 (Villaver et al. 2004), and Dopita & Meatheringham (1991) for all other PNe. Estimated progenitor masses M_{init} are from Villaver et al. (2003, 2004).
[d] N/O ratio from Dopita & Meatheringham (1991).

LMC SMP 73 and SMC SMP 15. We nodded along the slit in ABBA sequences for maximum observing efficiency. The data were reduced using the FIREHOSE IDL reduction pipeline.[7] Th–Ar lamps were used to wavelength calibrate the spectra, and A0V standard stars were observed for each object to perform relative flux calibrations and telluric corrections.

LMC SMP 62 and SMC SMP 20 were observed in the *K* band with the Gemini Near-InfraRed Spectrograph (GNIRS) on the 8.1 m Gemini South telescope. We used the 111 l/mm grating in third order with a $0\farcs45 \times 99''$ slit, for an effective resolving power of $R = 4000$ in the wavelength range 2.1–2.3 μm. The data were taken in queue mode under observing program GS-2006B-Q-51. We beam-switched by nodding the target along the slit. The wavelength scale was established with an Ar arc lamp, and A0V standard stars were observed for flux calibration and telluric absorption corrections. The data were reduced using the FIGARO software package (Shortridge 1993). Fluxes and upper limits in the Gemini *K* band spectrum of SMP 20 agree well with our FIRE data, and we restrict our analysis to the FIRE data for this PN.

3. LINE MEASUREMENTS AND ABUNDANCE ANALYSIS

The FIRE spectra are very rich, with 80–110 emission lines detected in LMC objects and 60–85 in SMC PNe. We detect metal lines including [C I], [P II], [S II], [S III], [Fe III], [Kr III], and [Se IV], and several LMC PNe exhibit H_2 lines. We have also detected [Kr VI] 1.2333 μm[8] in LMC SMP 47 and SMP 99, and will discuss this identification in a forthcoming paper. Notably, Kr and/or Se were detected in all seven of the observed LMC PNe, and in one of the three SMC objects (Figure 1).

We measured line fluxes by integrating under the profile of each line above a local continuum using IDL routines, varying the continuum placement to estimate flux uncertainties. Gaussian fits were performed for blended features. We also measured 3σ upper limits to the [Rb IV] 1.5973, [Cd IV] 1.7203, and [Ge VI] 2.1930 μm lines identified by Sterling et al. (2016) and to [Se III] features. Line fluxes and intensities relative to H I Brγ are reported in Table 2.

For our abundance analysis, we adopt extinction coefficients, temperatures, densities, and ionic abundances used in ionization correction factors (ICFs) from the literature (see Table 1 for references). We adopt 10% uncertainties for He ionic abundances from the literature, and 30% for those of O and Ar. MD91 and LD06 do not report ionic abundances, and we derived these values from their listed intensities.

We calculated ionic and elemental abundances with the PyNeb analysis package (Luridiana et al. 2015), using the atomic data sources of García-Rojas et al. (2015, see their Table 5), with the exceptions of Rb^{3+}, Cd^{3+}, and Ge^{5+} for which we use the atomic data of Sterling et al. (2016). To minimize uncertainties due to errors in the flux calibration or adopted extinction coefficients, we computed ionic abundances relative to nearby H I lines: 11–3 for lines with wavelengths $\leqslant$1.0 μm, Paβ for the *J* band, Brζ for *H* band lines, and Brγ in the *K* band.

The [Se IV] 2.2864 μm line can be contaminated by H_2 3-2 S(2) 2.2870 μm in PNe with fluorescent H_2 emission (Dinerstein 2001), and this must be accounted for when computing Se^{3+}/H^+ abundances. The strengths of H_2 lines from the $v = 2$ and $v = 3$ levels in LMC SMP 47 and 85 are indicative of fluorescent excitation of moderately dense gas. For such conditions, the intensity of H_2 3-2 S(2) is about 0.8 times that of the 3-2 S(3) line (e.g., model 14 of Black & van Dishoeck 1987, for which $n = 3 \times 10^3$ cm^{-3}). We use these values to correct the measured fluxes at 2.287 μm for the contribution of H_2. The absence of the 3-2 S(3) line indicates that such corrections are not needed for the other PNe.

We report ionic abundances in Table 3. The error bars include uncertainties in the line fluxes, and assumed error bars of 1000 K in T_e and 20% for n_e values from the literature. All

[7] Available at http://web.mit.edu/~rsimcoe/www/FIRE/.
[8] All wavelengths reported in this Letter are vacuum wavelengths.

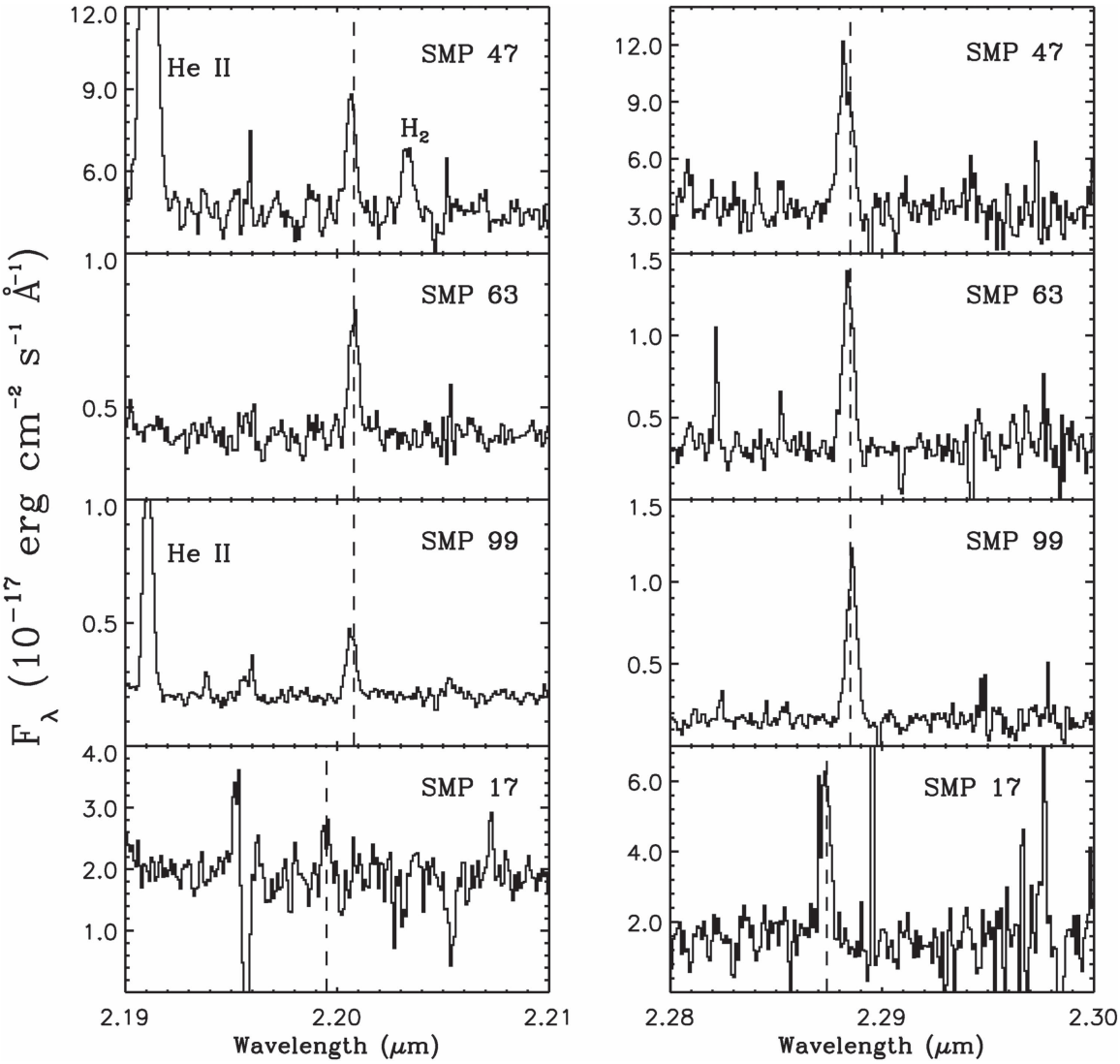

Figure 1. [Kr III] 2.1986 (left panels) and [Se IV] 2.2864 μm (right panels) detections in selected LMC PNe and SMC SMP 17. Vertical dashed lines correspond to the typical observed wavelength of each feature in LMC/SMC PNe.

abundance uncertainties were propagated via Monte Carlo simulations.

To convert ionic abundances to elemental abundances, we employ the ICF formulae of Delgado-Inglada et al. (2014) for light elements and those of Sterling et al. (2015, 2016) for *n*-capture elements. Uncertainties to the ICFs are the recommendations of Delgado-Inglada et al. (2014) for O, S, and Ar, and were propagated from the ionic and elemental abundances used in the ICF prescriptions for *n*-capture elements. In the case of the Kr ICF, we use Equation (1) of Sterling et al. (2015), which depends on S^{2+}/S, rather than Equation (2) (which uses Ar^{2+}/Ar), since [Ar III] lines were not detected in SMP 62 (LD06) and the derived Ar abundance in SMP 85 is larger than the solar value (Asplund et al. 2009) and appears to be inaccurate. The two equations produce Kr ICFs that agree to within 25% for our targets except for SMC SMP 20 (in which Kr is not detected), with no systematic trends. Therefore, this choice does not affect our results.

In Table 4, we give elemental abundances relative to the solar values of Asplund et al. (2009), with uncertainties accounting for those in the ionic abundances and ICFs. Our derived O abundances agree with literature values (MD91; T03; LD06; S10) to within 25% or better, while those for Ar show more scatter but agree to within 40% for most PNe. Our S abundances are factors of 2–14 lower than the values of LD06, in line with the findings of Bernard-Salas et al. (2008) and Shaw et al. (2010).

4. ABUNDANCE PATTERNS AND ENRICHMENTS

4.1. Evidence for Third Dredge-up and Choice of a Metallicity Reference

TDU conveys C-rich and *s*-process enriched material to the envelopes of AGB stars (Karakas & Lattanzio 2014), and therefore C-rich PNe can be expected to exhibit *s*-process enrichments. With the exceptions of LMC SMP 62 (Aller et al. 1987) and SMP 6 (no C abundance available), all PNe in our sample have C/O ratios of unity or larger, and thus experienced TDU.

To determine whether a PN is *s*-process enriched it is necessary to compare *n*-capture element abundances to that of an element representative of the metallicity [Fe/H], since Fe

Table 2
Line Identifications and Intensities

Line ID	Observed λ (μm)	Lab. λ (μm)	$F/F(\mathrm{Br}\gamma)$ ($\times$100)	$I/I(\mathrm{Br}\gamma)$ ($\times$100)	Comments
			LMC SMP 6		
H I	0.8368	0.8361	(3.66 ± 0.93)E+00	(6.59 ± 1.68)E+00	···
H I	0.8401	0.8395	(4.81 ± 1.09)E+00	(8.61 ± 1.94)E+00	···
H I	0.8447	0.8440	(8.56 ± 1.33)E+00	(1.52 ± 0.24)E+01	···
H I	0.8477	0.8470	(9.20 ± 1.47)E+00	(1.63 ± 0.26)E+01	···
H I	0.8513	0.8505	(1.07 ± 0.20)E+01	(1.89 ± 0.36)E+01	···
H I	0.8555	0.8548	(7.64 ± 1.70)E+00	(1.33 ± 0.30)E+01	···
H I	0.8608	0.8601	(1.16 ± 0.11)E+01	(2.00 ± 0.20)E+01	···

Note. Measured fluxes and intensities are on the scale $F(\mathrm{H\ I\ Br}\ \gamma) = I(\mathrm{H\ I\ Br}\ \gamma) = 100$. Marginal detections are marked with a colon.

(This table is available in its entirety in machine-readable form.)

abundances cannot be accurately determined in nebulae due to depletion into dust (e.g., Delgado-Inglada & Rodríguez 2014). In LMC field giants, α-elements such as O, Mg, Si, Ca, and Ti are approximately solar relative to Fe ($[\alpha/\mathrm{Fe}] = -0.1$ to 0.1) at the average LMC metallicity of $[\mathrm{Fe/H}] = -0.5$ (e.g., Lapenna et al. 2012; Van der Swaelmen et al. 2013). Similarly, in SMC red giants $[\alpha/\mathrm{Fe}] = 0.0$–0.1 (Mucciarelli 2014). Therefore, α-elements appear to be good tracers of [Fe/H] in these galaxies.

Of the α-species, oxygen is the most widely used metallicity tracer in PNe since its abundance is usually the most accurately determined. However, models of AGB nucleosynthesis predict that at low metallicities TDU can enrich O, although the amount of enrichment differs among different AGB evolutionary codes (e.g., Cristallo et al. 2015; Ventura et al. 2015; Karakas & Lugaro 2016). Furthermore, these calculations all show that for initial masses $\gtrsim 4\ M_{\odot}$, O can be depleted by the CNO cycle during hot bottom burning (HBB; H-burning at the base of the convective envelope).

LD06 found evidence for both O enrichment and destruction in a sample of 183 LMC and SMC PNe. We find similar effects in our abundance analysis. In several of our observed PNe, [O/(S, Ar)] = 0.2–0.4, indicating that TDU may have enhanced O in their progenitor stars. In contrast, the Type I PN LMC SMP 47, which likely experienced HBB based on its large N/O ratio (LD06), has subsolar [O/(S, Ar)], indicating that O depletion may have occurred. For some PNe, [O/(S, Ar)] is solar within the abundance uncertainties, but for uniformity we use S and Ar as tracers of [Fe/H] for all of our targets.

4.2. Neutron-capture Element Abundances

In assessing whether our targets are self-enriched by *s*-process nucleosynthesis, it should be noted that the initial abundances of *n*-capture elements in the progenitor stars of our sample may not follow the solar abundance pattern, due to the different star formation histories and chemical evolution of the Magellanic Clouds compared to the Milky Way. Various studies find different ratios of trans-iron element abundances relative to Fe in pre-AGB LMC stars. The case of the SMC appears simpler, if only because there are few *n*-capture element abundance determinations in its red giant stars.

Se, Kr, and Rb lie on or below the first ("light-*s*," or ls) *s*-process peak, but these elements have not been detected in the spectra of late-type stars in the LMC or SMC. Instead, we compare our results with Y and Zr, two light-*s* elements that are relatively well-studied in stars. Pompéia et al. (2008) found [ls/Fe] = −0.4 to −0.5 dex in inner-disk LMC stars, while [ls/Fe] is approximately solar in clusters (Colucci et al. 2012) and the disk stars investigated by Van der Swaelmen et al. (2013). For elements belonging to the second ("heavy-*s*," or hs) peak (e.g., La), abundances from the above studies give [hs/Fe] = 0.2–0.5. In SMC Cepheids, Luck et al. (1998) found that [ls/Fe] is slightly subsolar (−0.20 to −0.05 dex) while [hs/Fe] is 0.1–0.3 dex.

Based on this information, we consider Se, Kr, and Rb to be enriched in LMC and SMC PNe if their abundances relative to S or Ar are larger than solar. Kr is strongly enriched in all PNe in which it was detected, by 0.6 dex (SMP 63) to as much as 1.3 dex (SMP 85 and SMP 99) in LMC PNe, and by 0.6 dex in SMC SMP 17. Se is also enriched in five of the targets, by 0.5–0.9 dex in the LMC and 0.5 dex in SMP 17.

The derived Se and Kr enrichment factors in these PNe generally agree with model predictions for these metallicities (Cristallo et al. 2015; Karakas & Lugaro 2016). Given that these models predict that elements in the second *s*-process peak should be more strongly enriched at low metallicities than those in the first peak, the large Se and Kr enrichments indicate that even greater enhancements of heavier *n*-capture elements can be expected. While our nominal upper limits on [Cd/(S, Ar)] do not conform to this expectation, we note that our Cd abundances in two Galactic PNe are lower than predicted by models (Sterling et al. 2016), which suggests that the disagreement is likely due to uncertainties in the atomic data and/or ICF for this element.

The Type I PN LMC SMP 47 has both C/O and N/O ratios exceeding unity, suggesting that it experienced TDU after the cessation of HBB and has a progenitor mass $\sim 3.5\ M_{\odot} \leqslant M < 6\ M_{\odot}$ (Ventura et al. 2015). The Rb abundance can also place limits on the progenitor mass, since this element can be strongly enriched if $^{22}\mathrm{Ne}(\alpha, n)^{25}\mathrm{Mg}$ dominates neutron production (García-Hernández et al. 2009; Karakas et al. 2012) as opposed to $^{13}\mathrm{C}(\alpha, n)^{16}\mathrm{O}$, the neutron source in less massive AGB stars. SMP 47 shows no significant enrichment of Rb, indicating that the ^{13}C source dominated neutron production in its progenitor and that its initial mass is $\lesssim 5.5\ M_{\odot}$ (Karakas & Lugaro 2016). This limit agrees with the predictions of Ventura et al. (2015).

The fact that the distances to the Magellanic Clouds are well known enables us to study the enrichment patterns as a function of PN luminosity and progenitor mass. Since this is a

Table 3
Ionic Abundances and Ionization Correction Factors

	LMC SMP 6	LMC SMP 47	LMC SMP 62 (GNIRS)	LMC SMP 63	LMC SMP 73	LMC SMP 85	LMC SMP 99	SMC SMP 15	SMC SMP 17	SMC SMP 20
Derived Ionic Abundances										
S^{+}/H^{+}	(1.9 ± 1.0)E−07	(3.6 ± 1.5)E−07	(3.6 ± 1.1)E−07[a]	(1.2 ± 0.9)E−07	(4.9 ± 3.3)E−07	(1.8 ± 1.3)E−07	(2.1 ± 1.3)E−07	(2.5 ± 2.0)E−07	(1.2 ± 0.6)E−07	(2.7 ± 1.6)E−08
S^{2+}/H^{+}	(1.2 ± 0.2)E−06	(2.7 ± 0.4)E−06	(8.1 ± 2.4)E−07[a]	(1.7 ± 0.4)E−06	(2.0 ± 0.5)E−06	(1.4 ± 0.3)E−06	(1.5 ± 0.3)E−06	(1.4 ± 0.3)E−06	(1.0 ± 0.3)E−06	(2.5 ± 0.4)E−07
Ge^{5+}/H^{+}	⩽6.6E−11	⩽3.3E−10	⩽2.4E−10	⩽1.4E−10	⩽2.2E−10	⩽1.9E−10	⩽1.5E−10	⩽2.2E−10	⩽5.5E−11	⩽1.5E−10
Se^{2+}/H^{+}	⩽1.0E−09	⩽1.4E−09	…	⩽4.7E−09	⩽9.1E−09	⩽6.6E−09	⩽2.9E−09	⩽7.9E−09	⩽1.2E−09	⩽1.2E−09
Se^{3+}/H^{+}	(7.2 ± 1.0)E−10	(1.9 ± 0.6)E−10	(7.4 ± 2.6)E−11	(7.2 ± 0.8)E−10	(1.9 ± 0.3)E−09	(3.1 ± 0.9)E−10	(2.0 ± 0.2)E−09	⩽3.4E−11	(7.5 ± 1.9)E−10	⩽2.4E−11
Kr^{2+}/H^{+}	(7.7 ± 1.6)E−10	(1.5 ± 0.3)E−10	⩽3.6E−10	(8.7 ± 1.4)E−10	⩽5.8E−10	(2.6 ± 0.7)E−09	(2.2 ± 0.2)E−09	⩽3.1E−10	(3.7 ± 1.3)E−10	⩽2.4E−10
Rb^{3+}/H^{+}	⩽1.6E−10	⩽2.3E−10	…	⩽3.7E−10	⩽8.7E−09	⩽4.1E−10	⩽3.2E−10	⩽9.8E−10	⩽8.8E−11	⩽1.9E−10
Cd^{3+}/H^{+}	⩽5.7E−11	⩽1.2E−10	…	⩽1.4E−10	⩽7.6E−10	⩽2.3E−10	⩽1.6E−10	⩽4.6E−10	⩽1.2E−10	⩽7.7E−11
Ionic Abundances from the Literature and ICFs[b]										
He^{+}/H^{+}	(6.0 ± 0.6)E−02	(8.2 ± 0.8)E−02	(7.3 ± 0.7)E−02	(1.1 ± 0.1)E−01	(7.0 ± 0.7)E−02	(7.6 ± 0.8)E−02	(8.8 ± 0.9)E−02	(9.3 ± 0.9)E−02	(1.4 ± 0.1)E−01	(1.4 ± 0.1)E−01
He^{2+}/H^{+}	(3.9 ± 0.4)E−02	(3.8 ± 0.4)E−02	(2.5 ± 0.3)E−02	(3.0 ± 0.3)E−04	(2.2 ± 0.2)E−02	…	(2.1 ± 0.2)E−02	(2.3 ± 0.2)E−02	(1.0 ± 0.1)E−03	…
O^{+}/H^{+}	(4.9 ± 1.5)E−05	(9.7 ± 2.9)E−06	(8.5 ± 2.5)E−06	(4.5 ± 1.3)E−06	(3.1 ± 0.9)E−05	(5.0 ± 1.5)E−05	(3.1 ± 0.9)E−05	(6.7 ± 2.0)E−06	(6.8 ± 2.0)E−06	(2.0 ± 0.6)E−06
O^{2+}/H^{+}	(1.6 ± 0.5)E−04	(1.1 ± 0.3)E−04	(1.0 ± 0.3)E−04	(1.9 ± 0.6)E−04	(3.1 ± 0.9)E−04	(7.6 ± 2.3)E−05	(2.0 ± 0.6)E−04	(1.1 ± 0.3)E−04	(1.6 ± 0.5)E−04	(5.4 ± 1.6)E−05
Ar^{2+}/H^{+}	(3.4 ± 1.0)E−07	(6.6 ± 2.0)E−07	…	(6.4 ± 1.9)E−07	(6.4 ± 1.9)E−07	(3.4 ± 1.0)E−07	(5.8 ± 1.7)E−07	(2.9 ± 0.9)E−07	(2.6 ± 0.8)E−07	(1.0 ± 0.3)E−07
ICF(O)	1.38 ± 0.27	1.27 ± 0.21	1.19 ± 0.17	1.00	1.18 ± 0.16	1.00	1.13 ± 0.13	1.14 ± 0.14	1.00	1.00
ICF(Ar)	1.68 ± 1.09	1.89 ± 1.22	…	1.68 ± 1.09	1.72 ± 1.12	1.08 ± 0.71	1.54 ± 1.00	1.77 ± 1.15	1.61 ± 1.05	1.62 ± 1.06
ICF(S)	1.55 ± 0.27	2.06 ± 0.33	1.97 ± 0.31	2.24 ± 0.36	1.84 ± 0.30	1.00	1.54 ± 0.25	2.06 ± 0.33	1.95 ± 0.31	1.00
ICF(Se)	2.98 ± 2.15	2.09 ± 1.72	1.91 ± 1.55	1.37 ± 1.48	1.92 ± 1.74	2.67 ± 1.78	1.95 ± 1.78	1.73 ± 1.44	1.42 ± 1.63	1.40 ± 1.18
ICF(Kr)	2.83 ± 1.74	3.73 ± 2.01	4.58 ± 3.70	3.85 ± 2.61	3.66 ± 2.51	1.64 ± 0.58	2.74 ± 1.65	3.88 ± 2.38	3.46 ± 2.39	1.59 ± 0.47
ICF (Rb, Cd)	1.80 ± 0.78	1.38 ± 0.61	…	1.02 ± 0.43	1.30 ± 0.56	1.65 ± 0.61	1.31 ± 0.54	1.20 ± 0.52	1.05 ± 0.44	1.04 ± 0.43

Notes.
[a] Derived from LD06 intensities.
[b] See the text.

Table 4
Elemental Abundances

	LMC SMP 6	LMC SMP 47	LMC SMP 62	LMC SMP 63	LMC SMP 73	LMC SMP 85	LMC SMP 99	SMC SMP 15	SMC SMP 17	SMC SMP 20
[O/H]	-0.23 ± 0.12	-0.50 ± 0.12	-0.57 ± 0.12	-0.39 ± 0.11	-0.09 ± 0.12	-0.59 ± 0.08	-0.28 ± 0.11	-0.55 ± 0.12	-0.48 ± 0.11	-0.95 ± 0.11
[S/H]	-0.80 ± 0.17	-0.32 ± 0.17	-0.76 ± 0.18	-0.52 ± 0.18	-0.46 ± 0.18	-0.92 ± 0.08	-0.70 ± 0.19	-0.59 ± 0.18	-0.77 ± 0.18	-1.68 ± 0.06
[Ar/H]	-0.65 ± 0.26	-0.30 ± 0.26	…	-0.37 ± 0.26	-0.36 ± 0.26	0.17 ± 0.25	-0.45 ± 0.26	-0.69 ± 0.26	-0.78 ± 0.26	-1.18 ± 0.26
[Se/H]	-0.01 ± 0.25	-0.74 ± 0.30	-1.19 ± 0.30	-0.35 ± 0.27	0.21 ± 0.29	-0.43 ± 0.24	0.25 ± 0.24	$\leqslant -1.57$	-0.32 ± 0.32	$\leqslant -1.82$
[Se/S]	0.80 ± 0.28	-0.42 ± 0.33	-0.43 ± 0.33	0.17 ± 0.30	0.67 ± 0.32	0.50 ± 0.25	0.95 ± 0.28	$\leqslant -0.97$	0.45 ± 0.34	$\leqslant -0.14$
[Se/Ar]	0.64 ± 0.33	-0.44 ± 0.36	…	0.02 ± 0.34	0.57 ± 0.35	-0.59 ± 0.32	0.70 ± 0.32	$\leqslant -0.87$	0.47 ± 0.37	$\leqslant -0.64$
[Kr/H]	0.09 ± 0.22	0.49 ± 0.20	$\leqslant -0.04$	0.27 ± 0.23	$\leqslant 0.08$	0.38 ± 0.16	0.52 ± 0.21	$\leqslant -0.17$	-0.15 ± 0.25	$\leqslant -0.67$
[Kr/S]	0.89 ± 0.26	0.81 ± 0.24	$\leqslant 0.72$	0.79 ± 0.27	$\leqslant 0.53$	1.30 ± 0.17	1.23 ± 0.26	$\leqslant 0.42$	0.62 ± 0.29	$\leqslant 1.01$
[Kr/Ar]	0.74 ± 0.31	0.80 ± 0.30	…	0.64 ± 0.32	$\leqslant 0.44$	0.21 ± 0.28	0.97 ± 0.31	$\leqslant 0.52$	0.63 ± 0.33	$\leqslant 0.51$
[Rb/H]	$\leqslant -0.07$	$\leqslant -0.01$	…	$\leqslant 0.06$	$\leqslant 0.53$	$\leqslant 0.31$	$\leqslant 0.10$	$\leqslant 0.55$	$\leqslant -0.56$	$\leqslant -0.23$
[Rb/S]	$\leqslant 0.73$	$\leqslant 0.30$	…	$\leqslant 0.58$	$\leqslant 0.99$	$\leqslant 1.23$	$\leqslant 0.80$	$\leqslant 1.14$	$\leqslant 0.21$	$\leqslant 1.45$
[Rb/Ar]	$\leqslant 0.58$	$\leqslant 0.29$	…	$\leqslant 0.43$	$\leqslant 0.89$	$\leqslant 0.14$	$\leqslant 0.54$	$\leqslant 1.25$	$\leqslant 0.22$	$\leqslant 0.95$
[Cd/H]	$\leqslant 0.30$	$\leqslant 0.49$	…	$\leqslant 0.44$	$\leqslant 1.28$	$\leqslant 0.87$	$\leqslant 0.60$	$\leqslant 1.03$	$\leqslant 0.38$	$\leqslant 0.19$
[Cd/S]	$\leqslant 1.11$	$\leqslant 0.80$	…	$\leqslant 0.96$	$\leqslant 1.74$	$\leqslant 1.79$	$\leqslant 1.31$	$\leqslant 1.62$	$\leqslant 1.15$	$\leqslant 1.87$
[Cd/Ar]	$\leqslant 0.95$	$\leqslant 0.79$	…	$\leqslant 0.81$	$\leqslant 1.64$	$\leqslant 0.70$	$\leqslant 1.05$	$\leqslant 1.73$	$\leqslant 1.16$	$\leqslant 1.37$

Note. Abundances $[X/H] = \log(X/H)_{PN} - \log(X/H)_{\odot}$, computed from the ionic abundances and ICFs in Table 3.

brightness-limited sample, we preferentially selected objects at the bright end of the PNLF, whose formation mechanism has been widely debated (e.g., Ciardullo et al. 2005 and references therein). The substantial Se and especially Kr enrichments in the LMC PNe[9] are consistent with the interpretation (based on single-star evolution) that such bright PNe are primarily produced by stars with initial masses of 2–3 $M_{\odot}$ (which are expected to have the largest *s*-process enrichments; e.g., Cristallo et al. 2015; Karakas & Lugaro 2016). The estimated progenitor mass (1.5–2.0 $M_{\odot}$) for SMP 63 (Villaver et al. 2003) approximately agrees with this interpretation, but progenitor masses for our other LMC targets are unknown. Interestingly, this result seems to be at odds with the statistical analysis of Badenes et al. (2015), who found that the most luminous PNe in the LMC ($L_{5007} \geqslant 4 \times 10^{34}$ erg s^{-1}, corresponding to $m_{5007} \leqslant 18.44$) predominantly arise from stars with initial masses 1.0–1.2 $M_{\odot}$. Binary star formation mechanisms cannot be dismissed for luminous PNe (e.g., Ciardullo et al. 2005), but comparisons of CNO abundances to nucleosynthesis models (Ventura et al. 2015) and the progenitor masses computed by Villaver et al. (2003, 2007) provide evidence for a range of initial stellar masses (from ∼1 $M_{\odot}$ to as high as 6–8 $M_{\odot}$) for LMC PNe within a few magnitudes of the bright cutoff. Our current sample is too small to support strong conclusions regarding progenitor mass distributions. Determinations of *s*-process enhancements in a larger number of Magellanic Cloud PNe are needed for statistically meaningful constraints on the progenitors of luminous PNe in gas-rich galaxies.

We find no significant correlations between *s*-process enrichments and other nebular and stellar parameters, including C/O and N/O, central star temperature, and progenitor mass. The small size of our sample clearly limits our ability to test these relations, but the success of our observations demonstrates that it is feasible to expand this study to other PNe in the Magellanic Clouds. The *James Webb Space Telescope* will enable such investigations to be extended to more distant Local Group galaxies, as well as to PNe well below the bright cutoff of the PNLF in these systems.

We thank the anonymous referee, whose helpful suggestions improved this paper. We are grateful to M. Reiter and R. Simcoe for their valuable advice regarding the reduction of FIRE data, and to J. Wood for her role in obtaining the Gemini data. N.C.S. acknowledges support from the NSF through award AST-0901432, and I.U.R. acknowledges partial support from NSF grant PHY 14-30152 (Physics Frontier Center/JINA-CEE). The Gemini Observatory is operated by the Association of Universities for Research in Astronomy, Inc., under a cooperative agreement with the NSF on behalf of the Gemini partnership: the National Science Foundation (United States), the National Research Council (Canada), CONICYT (Chile), Ministerio de Ciencia, Tecnología e Innovación Productiva (Argentina), and Ministério da Ciência, Techologia e Inovação (Brazil). This work has made use of NASA's Astrophysics Data System and the FRUITY Database of nucleosynthetic yields from AGB stars (fruity.oateramo.inaf.it).

[9] Due to the detection of Se and Kr in just one SMC PN, a similar conclusion cannot be drawn at present for the SMC.

REFERENCES

Aller, L. H., Keyes, C. D., Maran, et al. 1987, ApJ, 320, 159
Asplund, M., Grevesse, N., Sauval, A. J., & Scott, P. 2009, ARA&A, 47, 481
Badenes, C., Maoz, D., & Ciardullo, R. 2015, ApJL, 804, L25
Bernard-Salas, J., Pottasch, S. R., Gutenkunst, S., Morris, P. W., & Houck, J. R. 2008, ApJ, 672, 274
Black, J. H., & van Dishoeck, E. F. 1987, ApJ, 322, 412
Ciardullo, R., Sigurdsson, S., Feldmeier, J. J., & Jacoby, G. H. 2005, ApJ, 629, 499
Colucci, J. E., Bernstein, R. A., Cameron, S. A., & McWilliam, A. 2012, ApJ, 746, 29
Cristallo, S., Straniero, O., Piersanti, L., & Gobrecht, D. 2015, ApJS, 219, 40
Delgado-Inglada, G., Morisset, C., & Stasińska, G. 2014, MNRAS, 440, 536
Delgado-Inglada, G., & Rodríguez, M. 2014, ApJ, 784, 173
Dinerstein, H. L. 2001, ApJL, 550, L223
Dopita, M. A., & Meatheringham, S. J. 1991, ApJ, 377, 480 (MD91)
Dopita, M. A., Vassiliadis, E., Meatheringham, S. J., et al. 1994, ApJ, 426, 150
Drašković, D., Parker, Q. A., Reid, W. A., & Stupar, M. 2015, MNRAS, 452, 1402
Frew, D. J., Parker, Q. A., & Bojičić, I. S. 2016, MNRAS, 455, 1459
García-Hernández, J. I., Iglesias-Groth, S., Rebolo, R., et al. 2009, ApJ, 706, 866
García-Rojas, J., Madonna, S., Luridiana, V., et al. 2015, MNRAS, 452, 2606
Jacoby, G. H. 1989, ApJ, 339, 39
Karakas, A. I., García-Hernández, D. A., & Lugaro, M. 2012, ApJ, 751, 8
Karakas, A. I., & Lattanzio, J. C. 2014, PASA, 31, 30
Karakas, A. I., & Lugaro, M. 2016, ApJ, 825, 26
Karakas, A. I., van Raai, M. A., Lugaro, M., Sterling, N. C., & Dinerstein, H. L. 2009, ApJ, 690, 1130
Keller, S. C., & Wood, P. R. 2006, ApJ, 642, 834
Lapenna, E., Mucciarelli, A., Origlia, L., & Ferraro, F. R. 2012, ApJ, 761, 33
Leisy, P., & Dennefeld, M. 2006, A&A, 456, 451 (LD06)
Luck, R. E., Moffett, T. J., Barnes, T. G., III, & Gieren, W. P. 1998, AJ, 115, 605
Luridiana, V., Morisset, C., & Shaw, R. A. 2015, A&A, 573, 42
Meatheringham, S. J., & Dopita, M. A. 1991, ApJS, 76, 1085
Mucciarelli, A. 2014, AN, 335, 79
Otsuka, M., Meixner, M., Riebel, D., et al. 2011, ApJ, 729, 39
Péquignot, D., & Baluteau, J. P. 1994, A&A, 283, 593
Pompéia, L., Hill, V., Spite, M., et al. 2008, A&A, 480, 379
Reid, W. A. 2014, MNRAS, 438, 2642
Sharpee, B., Zhang, Y., Williams, R., et al. 2007, ApJ, 659, 1265
Shaw, R. A., Lee, T.-H., Stanghellini, L., et al. 2010, ApJ, 717, 562 (S10)
Shaw, R. A., Stanghellini, L., Villaver, E., & Mutchler, M. 2006, ApJS, 167, 201
Shortridge, K. 1993, in ASP Conf. Ser. 52, Astronomical Data Analysis Software and Systems II, ed. R. J. Hanisch, R. J. V. Brissenden, & J. Barnes (San Francisco, CA: ASP), 219
Simcoe, R. A., Burgasser, A. J., Schechter, P. L., et al. 2013, PASP, 125, 270
Stanghellini, L., Lee, T.-H., Shaw, R. A., Balick, B., & Villaver, E. 2009, ApJ, 702, 733
Stanghellini, L., Shaw, R. A., Balick, B., et al. 2003, ApJ, 596, 997
Sterling, N. C., & Dinerstein, H. L. 2008, ApJS, 174, 158
Sterling, N. C., Dinerstein, H. L., Kaplan, K. F., & Bautista, M. A. 2016, ApJL, 819, L9
Sterling, N. C., Porter, R. L., & Dinerstein, H. L. 2015, ApJS, 218, 25
Tsamis, Y. G., Barlow, M. J., Liu, X.-W., Danziger, I. J., & Storey, P. J. 2003, MNRAS, 345, 186 (T03)
Van der Swaelmen, M., Hill, V., Primas, F., & Cole, A. A. 2013, A&A, 560, 44
Ventura, P., Stanghellini, L., Dell'Agli, F., García-Hernández, D. A., & Di Criscienzo, M. 2015, MNRAS, 452, 3679
Villaver, E., Stanghellini, L., & Shaw, R. A. 2003, ApJ, 597, 298
Villaver, E., Stanghellini, L., & Shaw, R. A. 2004, ApJ, 614, 716
Villaver, E., Stanghellini, L., & Shaw, R. A. 2007, ApJ, 656, 831
Wood, J. L., Dinerstein, H. L., Geballe, T. R., & Sterling, N. C. 2006, BAAS, 38, 1113